RSC Chemical Biology

ROYAL SOCIETY OF CHEMISTRY

PAPER

View Article Online
View Journal | View Issue

Cite this: *RSC Chem. Biol.*, 2025, **6**, 1089

RaPID discovery of cell-permeable helical peptide inhibitors con-taining cyclic β-amino acids against SARS-CoV-2 main protease†

Marina Kawai,[a] Tika R. Malla,[b] H. T. Henry Chan,[c] Anthony Tumber,[b] Lennart Brewitz,[b] Eidarus Salah,[b] Naohiro Terasaka,[a] Takayuki Katoh,[a] Akane Kawamura,[bd] Christopher J. Schofield,[b] Fernanda Duarte[c] and Hiroaki Suga*[a]

Structurally constrained cyclic β-amino acids are attractive building blocks for peptide drugs because they induce unique and stable conformations. Introduction of (1*S*,2*S*)-2-aminocyclopentanecarboxylic acid [(1*S*,2*S*)-2-ACPC] into peptides stabilizes helical conformations, so improving proteolytic stability and cell membrane permeability. We report on the ribosomal synthesis of a helical peptide library incorporating (1*S*,2*S*)-2-ACPC at every third position and its application for the discovery of SARS-CoV-2 main protease (M^{pro}) inhibitors. We identified two peptide sequences containing multiple (1*S*,2*S*)-2-ACPC residues, which exhibit helical conformations and superior proteolytic stability compared with their α-Ala or β-Ala counterparts. Studies using the chloroalkane cell-penetration assay showed that their cell permeability values (CP_{50}) are comparable with or even slightly better than that of the cell-penetrating nona-arginine (R9) peptide. The new approach is thus a highly efficient method that combines a helical peptide library containing structurally constrained cyclic β-amino acids with the classical RaPID discovery method, enabling *de novo* discovery of proteolytically stable and cell-penetrating bioactive peptides that target intracellular proteins.

Received 2nd February 2025,
Accepted 2nd May 2025

DOI: 10.1039/d5cb00021a

rsc.li/rsc-chembio

Introduction

Helical structures are often observed in bioactive cell-penetrating peptides (CPPs). For example, melittin, found in the genus *Apis*, interacts with cell membranes and forms pores in lipid bilayers owing to its amphipathic α-helical structure.[1,2] The α-helicity of melittin enables it to form a rigid binding interface that interacts with its target protein, calmodulin, resulting in potent inhibition of tumor cell proliferation.[3–5] Therefore, helical peptides are an attractive class of peptides for developing probes against intracellular protein targets.

In general, short peptides comprised solely of α-amino acids (α-peptides) are unable to fold into stable helical structures due to their flexible backbones; >20 residues are typically required for formation of stable helices.[6] Various strategies for stabilizing helical peptide structures have been developed. For example, side-chain-to-side-chain covalent bridges can be introduced for stabilization of helices to develop α-helix-mediated protein–protein interaction inhibitors based on rational or semi-rational designs.[7]

By contrast with α-amino acids, structurally constrained cyclic $\beta^{2,3}$-amino acids (cβAAs) can form well-defined, stable secondary structures in short peptides,[8] which are often referred to as foldamers.[9] (1*S*,2*S*)-2-Aminocyclopentanecarboxylic acid [(1*S*,2*S*)-2-ACPC] is a cβAA which strongly enhances the helical propensity of peptides when combined with α-amino acids (α/β-peptides),[10,11] in a largely side chain independent manner. In particular, introduction of (1*S*,2*S*)-2-ACPC at every third residue gives rise to unique helical structures such as 10/11/11-helix and 14-helix conformations (Fig. 1).[12,13] 10/11/11-helix is characterized by an $i \rightarrow i + 3$ hydrogen bonding pattern, whereas 14-helix adopts an $i \rightarrow i + 4$ hydrogen bonding pattern, which is similar to that of the α-helix (also referred to as a 13-helix). Such α/β-helical peptides are

[a] *Department of Chemistry, Graduate School of Science, The University of Tokyo, Tokyo, Japan*
[b] *Department of Chemistry and the Ineos Oxford Institute for Antimicrobial Research, Chemistry Research Laboratory, University of Oxford, 12 Mansfield Road, Oxford OX1 3TA, UK*
[c] *Physical and Theoretical Chemistry Laboratory, University of Oxford, South Parks Road, Oxford OX1 3QZ, UK*
[d] *Chemistry – School of Natural and Environmental Sciences, Newcastle University, Newcastle upon Tyne, UK*

† Electronic supplementary information (ESI) available. See DOI: https://doi.org/10.1039/d5cb00021a

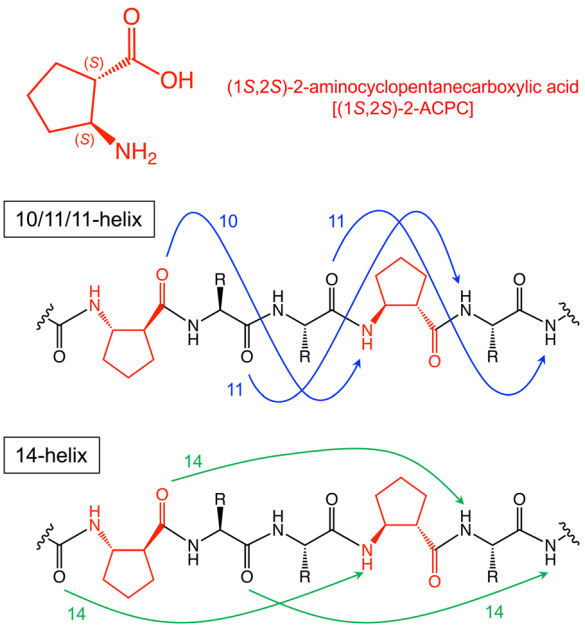

Fig. 1 Structure of (1*S*,2*S*)-2-aminocyclopentanecarboxylic acid and models of hydrogen-bond patterns that define 10/11/11-helix and 14-helix. Reported *i*, *i* + 3 C═O···H–N hydrogen bonds are in blue (10/11/11-helix), and *i*, *i* + 4 C═O···H–N hydrogen bonds are in green (14-helix).

anticipated to have high rigidity and compactness, properties that can be advantageous both for cell membrane permeation and strong binding to target molecules. Importantly, such cβAAs also potentially decrease susceptibility to proteolysis owing to their unnatural backbones.[14] Thus, cβAAs are attractive building blocks for the development of structurally and biologically stable bioactive peptides targeting intracellular proteins, including for drug development. To date, reported helical α/β-peptides have been the result of rational or semi-rational designs, based on knowledge of how the parental α-peptides interact with the target proteins.[15,16]

Ribosomal translation of non-proteinogenic α-amino acids has been achieved by means of a custom-made *Escherichia coli* translation system in the combination with the flexizyme technology, referred to as the flexible *in vitro* translation system (FIT system).[17,18] Although ribosomally mediated multiple incorporation of β-amino acids was once extremely difficult due to the slow accommodation of β-aminoacyl-tRNA to the ribosomal A-site and slow peptidyl transfer, this limitation has been recently overcome by devising a new class of engineered tRNA, named $tRNA^{Pro1E2}$.[19,20] This tRNA has a chimeric structure consisting of T-stem derived from $tRNA^{Glu}$ possessing a higher binding affinity to EF-Tu,[21,22] and D-arm derived from $tRNA^{Pro1}$ capable of binding to EF-P,[23] respectively. The use of β-aminoacyl-$tRNA^{Pro1E2}$ enhances its accommodation efficiency to the A site mediated by EF-Tu and peptidyl transfer reaction of peptidyl-$tRNA^{Pro1E2}$ mediated by EF-P, resulting in higher incorporation efficiency of β-amino acids. As a result, multiple incorporations of cβAA repertoires have become possible,[24–26] prompting us to construct diverse peptide libraries containing multiple cβAAs.

The application of such libraries to the Random non-standard Peptides Integrated Discovery (RaPID) system, built based on mRNA display,[27] has led to the discovery of *de novo* macrocycle inhibitors, F3 and F4, against human FXIIa.[25] A co-crystal structure of FXIIa with F3 containing two residues of (1*S*,2*S*)-2-aminocyclohexanecarboxylic acid (ACHC) revealed that it has a unique β-sheet-like macrocyclic structure, wherein the ACHC residues enable significant structural stabilization of the macrocycle. Remarkably, the cyclohexane rings of the ACHCs also interact directly with the specific hydrophobic residues of FXIIa, contributing to not only high resistance against serum proteases (with a half-life of 60 h) but also to the strong binding ability of F3.

Encouraged by the above success, it occurred to us that a *de novo* α/β-helical peptide library can be built if the placement of (1*S*,2*S*)-2-ACPC is achieved at periodic positions in peptide sequences under the reprogrammed genetic code. Here we report ribosomal construction of (1*S*,2*S*)-2-ACPC-containing helical peptide libraries, which were used for the RaPID selection against the SARS-CoV-2 main protease (M^{pro}) to discover *de novo* α/β-helical peptide inhibitors with favorable serum peptidase resistance and membrane permeability properties.

Results

Ribosomal synthesis of (1*S*,2*S*)-2-ACPC-containing helical peptide libraries

The flexizyme technology afforded essential aminoacyl-tRNAs for construction of α/β-helical libraries, where the initiator fMet (AUG) was reprogrammed to *N*-acetyl-L-tyrosine (Ac-L-Tyr) using an Ac-L-Tyr-$tRNA^{ini}_{CAU}$ while (1*S*,2*S*)-2-ACPC was assigned to the elongator Met (AUG) codon using a (1*S*,2*S*)-2-ACPC-$tRNA^{Pro1E2}_{CAU}$ (Fig. S1A and B, ESI†). The mRNA libraries encoding α/β-helical peptides with lengths of 7–15 residues were designed to have periodic AUG codons at every third position, introducing 2–5 residues of (1*S*,2*S*)-2-ACPC (Fig. 2A). Fifteen canonical amino acids (A, C, D, F, G, H, I, L, N, P, R, S, T, V, and Y) were assigned by the NNU codons, whereas unused amino acids (E, K, M, Q, and W) and the corresponding aminoacyl-tRNA synthetases (ARSs) were omitted to construct a FIT system for this particular setup.[17,18] A C-terminal TGVTNG sequence was introduced as a spacer connected to the 3′-end of the corresponding mRNA.

We previously observed that the multiple consecutive incorporations of β-amino acids suffered from poor translation efficiency depending on the type of β-amino acids.[20,25,28] Hence we first investigated if the translation efficiency and fidelity of the designed library would be sufficient to construct it. We designed a model peptide containing five (1*S*,2*S*)-2-ACPCs at every third position (Pcβ5) and attempted to express it using the custom-made FIT system (Fig. 2B). Analysis of the product using matrix-assisted laser desorption/ionization-time-of-flight mass spectrometry (MALDI-TOF MS) (Fig. 2C) showed only the expected monovalent ($[M + H]^+$) and divalent ($[M + 2H]^{2+}$) ions for Pcβ5. Based on experience, we considered that this level of

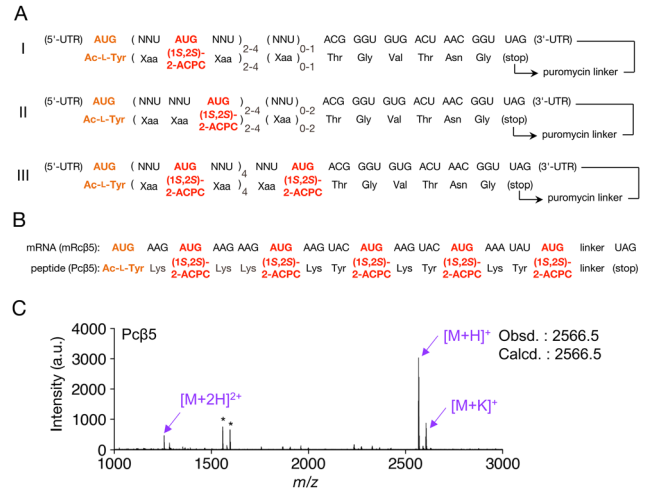

Fig. 2 Library designs of the (1*S*,2*S*)-2-ACPC-containing helical peptides. (A) Sequences of the mRNA libraries, I–III, coding α/β-helical peptide libraries containing random 4–10 NNU codons and the corresponding peptide sequences. The puromycin linker covalently links the respective mRNA to the translated peptide by ribosome catalysis. These mRNA libraries were combined into one mRNA library for the expression of a peptide library containing (1*S*,2*S*)-2-ACPC at the designated positions using the elongator AUG codon. (B) A model peptide, Pcβ5, and its mRNA template, mRcβ5. Pcβ5 was designed to contain five (1*S*,2*S*)-2-ACPCs at the designated positions assigned by the elongator AUG codon. (C) MALDI-TOF MS analysis of Pcβ5 expressed in the custom-made FIT system. Purple arrows indicate monovalent ($[M + H]^+$, and $[M + K]^+$) and divalent ($[M + 2H]^{2+}$) ions of Pcβ5, respectively. "Obsd." and "Calcd" denote observed and calculated *m*/*z* values of monovalent ion of Pcβ5, respectively. Asterisks (*) show unknown impurities, inherently present in the FIT system.

quality of translation should be sufficient for the expression of (1*S*,2*S*)-2-ACPC-containing peptides in a library format.

De novo discovery of (1*S*,2*S*)-2-ACPC-containing helical peptide ligands

Encouraged by the clean expression of the Pcβ5 peptide, we proceeded with a selection campaign using the (1*S*,2*S*)-2-ACPC-containing helical peptide libraries (Fig. S2A, ESI†). As a biomedicinally important intracellular target, we selected the SARS-CoV-2 main protease (M^{pro}), which is involved in the replication of the coronavirus.[29] The initial mRNA libraries I–III (Fig. 2A) were combined into a single mRNA library, which was then ligated to a puromycin-linked oligonucleotide, then subject to *in vitro* translation using the FIT system and reverse transcription to produce an mRNA/cDNA-tagged peptide library. The peptide library was then applied to naked streptavidin-coated magnetic beads to remove bead-binding peptides using three rigorous washes. The supernatant was then applied to biotinylated M^{pro}-immobilized beads for affinity-based M^{pro} screening. The recovered cDNA was amplified by PCR and transcribed for the next round of selection.

After the sixth and seventh rounds of the selection, the amount of recovered mRNA/cDNA-tagged peptides bound to M^{pro} substantially increased (Fig. S2B, ESI†). The recovered DNA sequences after the sixth and seventh rounds of the selection were analyzed by deep sequencing, leading to the identification of several families of enriched peptides (Table S2, ESI†).

Although the initial library was designed to have elongator AUG codons encoding (1*S*,2*S*)-2-ACPC at every third position, in the top 100 peptide sequences we found that the enriched peptides contained Ile-, Thr-, or Val-residues at the intended positions of (1*S*,2*S*)-2-ACPC (Table S2, ESI†). Such mutations could be introduced by PCR mutations, with the resulting peptides being translated more efficiently than the parental (1*S*,2*S*)-2-ACPC encoding peptides. The deep sequencing result suggests the plausible peptide sequences derived from the respective mRNA libraries as designed, except for **Mph2** (Table 1); **Mph2** has an extra α-amino acid at the N-terminus probably due to PCR mutations. It should be noted that no peptide was found from mRNA library III, probably because of its poorer expression level compared with mRNA library I and II, reducing the translation of the full-length peptides from mRNA library III. Based on the observed high read frequencies and the high numbers of (1*S*,2*S*)-2-ACPC appearing in their sequences, we chose peptides **Mph1–Mph6** for further analysis (Table 1).

Binding kinetics and inhibitory activity of selected peptides

Peptides **Mph1–6** were chemically synthesized (Fig. S3, ESI†) to evaluate binding affinity by surface plasmon resonance (SPR)

Table 1 Sequences and binding affinities of peptides obtained from deep sequencing after the sixth round of RaPID selection. Kinetic association (k_a) and dissociation (k_d) rates, and equilibrium (K_D) constant were determined by surface plasmon resonance. β, (1*S*,2*S*)-2-ACPC. —, the values could not be reliably determined due to poor 1 : 1 fitting

Originated library	Peptide	Sequence	Read (%) at 6th round	k_a (10^6 M^{-1} s^{-1})	k_d (10^{-2} s^{-1})	K_D (nM)
I	**Mph1**	^{Ac}YPβFGIVFβGHβCN-NH_2	14	—		
[a]	**Mph2**	^{Ac}YILFβGHβCSβRH-NH_2	2.6	—		
II	**Mph3**	^{Ac}YRFβRNβVFβFYβTD-NH_2	0.94	80.0	1.21	15.1
II	**Mph4**	^{Ac}YIPIRFβGHβCSβNN-NH_2	0.76	—		
I	**Mph5**	^{Ac}YDβFYβYVTFHVAT-NH_2	0.21	12.6	0.373	29.5
I	**Mph6**	^{Ac}YPβFGβVFβGHβCN-NH_2	0.02	—		

[a] The origin of library of **Mph2** was not determined from the cDNA sequence.

Table 2 Comparison of M^{pro} binding (1*S*,2*S*)-2-ACPC-containing peptides and their mutants in binding affinity, inhibitory activity, serum stability, and cell permeability. Kinetic association (k_a), dissociation (k_d), equilibrium (K_D) constants were measured by SPR. IC_{50} values were determined by solid-phase extraction coupled with mass spectrometry. The half-lives of peptides in human serum ($t_{1/2}$) were estimated by LC-MS. β, (1*S*,2*S*)-2-ACPC; B, β-Ala. —, the values could not be reliably determined. NT denotes "not tested"

Peptide	Sequence	k_a (10^6 M^{-1} s^{-1})	k_d (10^{-2} s^{-1})	K_D (nM)	IC_{50} (μM)	Serum half-life $t_{1/2}$ (h)	CP_{50} (nM)
Mph3	Ac-YRFβRNβVFβFYβTD-NH_2	80.0	1.21	15.1	0.62	2.4	340
Mph3A	Ac-YRFARNAVFAFYATD-NH_2	—	—	—	2.9	<10 min	1030
Mph3B	Ac-YRFBRNBVFBFYBTD-NH_2	—	—	—	>17	0.59	770
Mph3y	Ac-yRFβRNβVFβFYβTD-NH_2	65.2	0.576	8.83	0.96	11	240
Mph3-tr2	NH_2-βRNβVFβFYβTD-NH_2	—	—	—	5.2	>24 h	NT
Mph5	Ac-YDβFYβYVTFHVAT-NH_2	12.6	0.373	29.5	0.64	2.6	NT
Mph5A	Ac-YDAFYAYVTFHVAT-NH_2	—	—	—	>16	<10 min	NT
Mph5B	Ac-YDBFYBYVTFHVAT-NH_2	23.1	0.379	16.4	0.77	0.53	NT

(Table 1 and Fig. S4, ESI†). **Mph1**, **Mph2**, **Mph4**, and **Mph6** did not show reliable SPR fitting data (note that **Mph6** is identical to **Mph1** except for Ile6). On the other hand, **Mph3** and **Mph5** exhibited reliable fitting data; their K_D values were determined to be 15.1 and 29.5 nM, respectively. Therefore, we chose **Mph3** and **Mph5** for mutation studies to evaluate the contribution of (1*S*,2*S*)-2-ACPC to the binding affinity (Table 2 and Fig. S5, ESI†). Neither **Mph3A** nor **Mph3B** with quadruple substitutions manifested reliable binding kinetics with M^{pro}, indicating that the (1*S*,2*S*)-2-ACPC residues in **Mph3** are crucial for its excellent binding affinity. **Mph5A**, which contains the double α-Ala substitutions, also lost binding ability (K_D > 10 μM), whereas **Mph5B**, which contains the double β-Ala substitutions, exhibited a dissociation constant (K_D = 16.4 nM) comparable to **Mph5**. Thus, although the cyclopentane ring of (1*S*,2*S*)-2-ACPC in **Mph5** is not essential, it is critical to have β-amino acid residues at the relevant positions.

The M^{pro} inhibitory activities of **Mph3** and **Mph5** were measured by solid-phase extraction coupled with mass spectrometry (Table 2, Fig. S6, ESI†).[30] Variable concentrations of each peptide were co-incubated with an 11-mer M^{pro} substrate (TSAVLQ/SGFRK) and M^{pro}, and then both hydrolysis product and full-length substrate were quantified by the rapid-fire mass spectrometry. Inhibition of M^{pro} activity was evaluated by the percentage of substrate cleavage. Both peptides showed potent inhibitory activity with the IC_{50} values of 0.62 μM and 0.64 μM, respectively. On the other hand, **Mph3A** showed a ~5-fold reduced potency (2.9 μM), while **Mph3B** was only weakly active (>17 μM) (Table 2 and Fig. S6A, ESI†), observations which are consistent with the K_D measurement described above. As expected, **Mph5B** was able to inhibit with comparable potency (0.77 μM) to the parental **Mph5**, whereas **Mph5A** did not show inhibitory activity (Table 2 and Fig. S6B, ESI†).

Secondary structural analysis of Mph3 and Mph5

To evaluate the contribution of secondary structure elements of the peptides to binding affinity and inhibitory activity against M^{pro}, the peptides were analyzed by far-UV circular dichroism (CD) spectroscopy. Gellman and coworkers have reported that

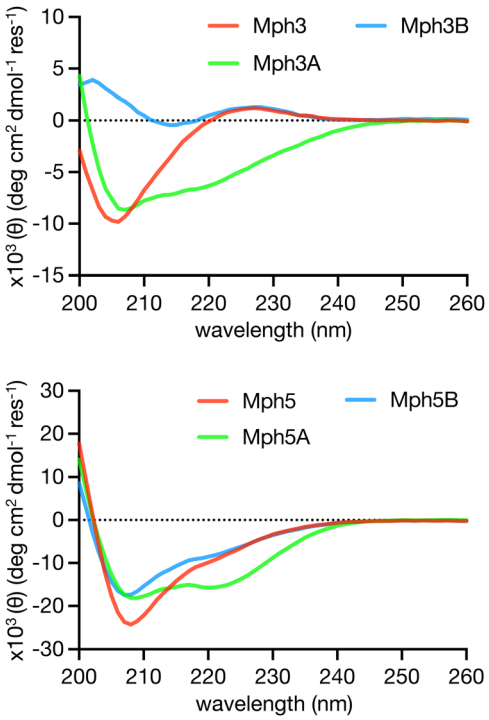

Fig. 3 Far-UV circular dichroism spectra of **Mph3**, **Mph3A**, **Mph3B** (top), and **Mph5**, **Mph5A**, **Mph5B** (bottom). Measurements were performed using 75 μM peptide in 50%$_{v/v}$ trifluoroethanol in 10 mM phosphate buffer (pH 8.0) at room temperature. Red lines, peptides obtained from the RaPID selection; green lines, α-Ala mutants; and blue lines, β-Ala mutants.

helical peptides containing cβAAs, such as 10/11/11-helix and 14-helix, are characterized by a single CD minimum at ~206 nm and similar to a mixture of α-helix and random coil,[31] while common α-helices have CD minima at 222 and 208 nm.[32] **Mph3** has a CD minimum at ~206 nm in 50%$_{v/v}$ trifluoroethanol (TFE) in phosphate buffer (pH 8.0), corresponding to the reported α/β-peptides with an ααβ pattern (Fig. 3). On the other hand, **Mph5**, that has an ααβ pattern at its N-terminus, showed a strong CD minimum at 208 nm and a weak shoulder at 222 nm, indicating that it likely has mixed

structural features involving both α/β-helix and weak α-helix conformations (Fig. 3). Note that TFE was used to improve the peptide solubility for the CD analysis. As TFE is known to stabilize helical structures,[33] the population of helix structures in 50%$_{v/v}$ TFE could be higher than that in water. Interestingly, **Mph1**, **Mph2**, **Mph4**, and **Mph6** all exhibited a single intense CD minimum at ~206 nm (Fig. S7, ESI†), indicating that their preferred secondary structures are α/β-helix regardless of poor binding ability to M^{pro}. These results imply that our library design enables production of the desired α/β-helical peptides.

We next analyzed the secondary structures of α-Ala and β-Ala mutants of **Mph3** and **Mph5** (Fig. 3). **Mph3A** showed a weak CD minimum at 208 nm and a weak shoulder at 222 nm, suggesting that a fraction of **Mph3A** is folded with an α-helical structure. **Mph5A** also showed a pronounced α-helical CD signature. This observation is consistent with the data that neither **Mph3A** nor **Mph3B** could retain the activity of their (1*S*,2*S*)-2-ACPC-containing parent (Table 2). Although **Mph3B** showed no signature of helicity, **Mph5B** showed a profile of helicity similar to the parental **Mph5**. Among the α-Ala/β-Ala-substituted analogs of **Mph3** and **Mph5**, only **Mph5B** exhibited a comparable inhibitory activity against M^{pro} to the parent peptide (**Mph5**), indicating that the α/β-helicity plays a critical role in efficient M^{pro} inhibition.

Proteolytic stability of the Mph3, Mph5, and mutants

We evaluated the proteolytic stability of **Mph3** and **Mph5**, as well as their α-Ala or β-Ala mutants, **Mph3A**, **Mph5A**, **Mph3B**, and **Mph5B** (Fig. 4). Each sample was co-incubated with an internal standard peptide in human serum at 37 °C. The quantity of remaining full-length peptides was estimated at each time point (0, 0.5, 1, 2, 4, 6, and 20 or 24 h) by liquid chromatography/mass spectrometry (LC–MS). The results reveal that **Mph3** and **Mph5** exhibited protease resistance with half-lives ($t_{1/2}$) of 2.4 and 2.6 h, respectively. Although these half-lives are not comparable to the reported α/β-peptides obtained from RaPID selection,[25] these $t_{1/2}$ values in serum were substantially higher than those of their α-Ala/β-Ala mutants ($t_{1/2}$ = <10 min for **Mph3A** and **Mph5A**, and 0.59 h and 0.53 h for **Mph3B** and **Mph5B**, respectively). This result well agrees with the earlier notion that the greater helical propensity owing to the cβAA residues could give rise to greater protease resistance in serum.[34,35]

The peptide bond cleavage sites of **Mph3** were analyzed by MALDI-TOF MS and LC–MS (Fig. S8, ESI†). After 20 h incubation in serum, 13-mer and 12-mer fragments, lacking the N-terminal ^{Ac}Y-R (**Mph3-tr1**) or ^{Ac}Y-R-F (**Mph3-tr2**) of **Mph3**, were observed by MALDI-TOF MS (Fig. S8A and B, ESI†). This observation suggested that the N-terminus of **Mph3** might be susceptible to peptidases present in serum. To validate the proteolytic stability of these fragments, **Mph3-tr1** and **Mph3-tr2** were chemically synthesized and tested for serum stability. Surprisingly, the half-life of **Mph3-tr1** was even shorter ($t_{1/2}$ = 0.38 h, Fig. S8C, ESI†) than that of **Mph3** ($t_{1/2}$ = 2.4 h), indicating that the Phe residue was rapidly removed from the N-terminus. On the other hand, **Mph3-tr2** was apparently

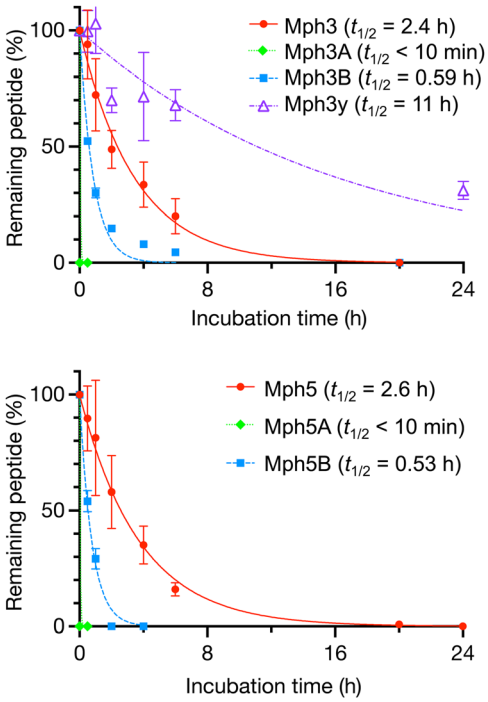

Fig. 4 Proteolytic stability of **Mph3**, **Mph3A**, **Mph3B**, **Mph3y** (top), and **Mph5**, **Mph5A**, **Mph5B** (bottom). The peptides were co-incubated with an internal standard peptide (NH_2-PEG_5-^{D}W^{D}S^{D}T^{D}N^{D}D^{D}W^{D}S^{D}T^{D}N^{D}D-PEG_5-$CONH_2$) in human serum for up to 20 h for (1*S*,2*S*)-2-ACPC mutants, and 24 h for **Mph3y**. The percentage of remaining peptides were estimated by LC/MS. Half-life ($t_{1/2}$) values were calculated using Prism8 GraphPad software. n = 3.

immune to peptidases over 24 h (Fig. S8C, ESI†), but a relatively large fluctuation of data and error range suggested that it might bind to serum proteins, such as albumin, possibly prohibiting peptidase digestions. To design an peptidase-resistant **Mph3** analog, we prepared **Mph3y**, whose N-terminal L-Tyr residue was substituted with the chiral counterpart D-Tyr (y). Notably, the Y1y substitution of **Mph3y** enhanced resistance to serum peptidases ($t_{1/2}$ = 11 h) by 4.6-fold compared with the parental **Mph3** ($t_{1/2}$ = 2.4 h).

We also evaluated the M^{pro} inhibitory activities of **Mph3-tr2** and **Mph3y** (Table 2 and Fig. S6A, S9, ESI†). **Mph3-tr2** showed a ~8-fold lower inhibitory activity (IC_{50} = 5.2 μM) than the full-length **Mph3** (IC_{50} = 0.62 μM). By contrast to **Mph3-tr2**, **Mph3y** exhibited similar levels of inhibition as **Mph3** (IC_{50} = 0.96 μM).

In summary, these studies reveal that the N-terminal ^{Ac}Y-R-F residues of **Mph3** play a role in exhibiting its M^{pro} inhibition activity, but these residues are susceptible to serum peptidases. Complete deletion of these residues increased their serum stability of the helical peptides but in turn caused detrimental loss of inhibitory activity. Alternatively, the Y1y substitution (**Mph3y**) improved the serum resistance without loss of inhibitory activity.

Cellular uptake of chloroalkane-labeled Mph3

Finally, we examined the cell permeability of the helical peptides by means of the chloroalkane penetration assay (CAPA)

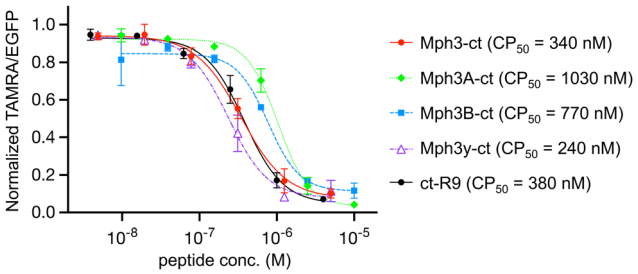

Fig. 5 Measurement of cell penetration using the chloroalkane penetration assay (CAPA). Each peptide with chloroalkane-tag (ct) was incubated with HaloTag-GFP-Mito cells in Opti-MEM for 24 h. The fluorescence of living cells and ct-TAMRA was detected and qualified by FACS. The data were normalized using peptide(−) control as 100% signal and peptide(−), ct-TAMRA(−) as 0% signal. CP_{50} values were calculated using Prism8 GraphPad software. n = 3.

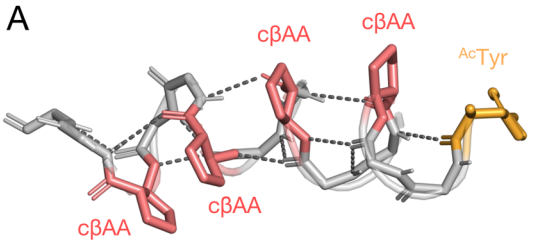

B

	Mph3	Mph3A	Mph3B
Clusters number	86	330	585
Population of top structure (%)	47	14	4
Polar contacts of top structure	11	4	4

Fig. 6 Structural calculation of the conformation of (1*S*,2*S*)-2-ACPC-containing peptides **Mph3**, **Mph3A**, and **Mph3B**. (A) A MD-generated structure of **Mph3**. (1*S*,2*S*)-2-ACPC is shown in pink and the initiator ^{Ac}Tyr in orange. Polar contacts are shown as dotted lines. (B) Comparison of structural clusters and enriched structures of **Mph3**, **Mph3A**, and **Mph3B**.

developed by the Kritzer group.[36] CAPA utilizes covalent bond formation between HaloTag protein and chloroalkane-tag for quantification of the cytosolic delivery of peptides. HEK293H cells expressing the HaloTag on the mitochondrial surface were pulsed with chloroalkane-tagged peptides (ct-peptides), followed by treatment with a chloroalkane-tagged fluorescent dye (ct-TAMRA). If the chloroalkane-tagged molecules permeate cells, they covalently bind to the HaloTag inside the cells *via* their chloroalkane-tag. Quantification of cell-permeated peptides was conducted by measuring fluorescence of ct-TAMRA that competes with ct-peptides. The chloroalkane-tag was conjugated to the C-terminus of peptides to minimize the false positive caused by peptidase degradation products (Fig. S10, ESI†). The conformations of C-terminal chloroalkane-tagged **Mph3** and its mutants (**Mph3-ct**, **Mph3A-ct**, **Mph3B-ct**, and **Mph3y-ct**, respectively) were similar to those of their parental peptides based on circular dichroism measurements (Fig. S11, ESI†). The potential cytotoxicity of **Mph3-ct** was also assessed using the Cell Counting Kit-8, showing no significant cytotoxicity even at 20 μM (Fig. S12, ESI†). For CAPA, cells were treated with 10, 40, 156, 625, 2500, and 10 000 nM of each ct-peptide for 22 h under 10% FBS conditions to determine a concentration at 50% cell permeation (CP_{50}). As a positive control, a well-studied polycationic CPP with an N-terminal chloroalkane-tag (**ct-R9**) was used in parallel at concentrations of 4, 15, 62.5, 250, 1000, and 4000 nM.

Remarkably, **Mph3-ct** exhibited a substantial cell membrane permeability with a CP_{50} values of 340 nM (Fig. 5), comparable to that of a positive control peptide, **ct-R9** (380 nM). Notably, the peptidase-resistant **Mph3y-ct** showed even better cell permeability with a CP_{50} value of 240 nM. In contrast, the CP_{50} values of **Mph3A-ct** and **Mph3B-ct** were approximately 3-fold and 2-fold higher (CP_{50} = 1030 nM and 770 nM, respectively) than that of **Mph3-ct**.

A possible reason for the observed better cell membrane permeability of **Mph3**/**3y-ct** over **Mph3A**/**3B-ct** is due to the pronounced helicity of **Mph3** observed by CD spectroscopy (Fig. 3), likely contributing to the compactness and low water coordination to the backbone. To substantiate this hypothesis, we performed molecular dynamics (MD) simulations to model the tertiary structure of **Mph3**, **Mph3A**, and **Mph3B**. The results imply that the most enriched (or abundant) structures of **Mph3** seems to be a 14-helix-like structure characterized by 11 polar contacts (Fig. 6A), with a cluster population of 47% (Fig. 6B). This suggests that **Mph3** may have a rigid helical structure and little chance of polar contacts with aqueous solution, both of which should be advantageous for improved cell permeation. In addition, hydrophobic side chains of (1*S*,2*S*)-2-ACPCs aligned along one face of the helical conformation, representing another structural feature that might have contributed to enhanced membrane permeability. In contrast, the most enriched structure of **Mph3A** was calculated as β-sheet-like structure characterized by 4 polar contacts, the cluster population of which was 14% (Fig. 6B). For **Mph3B**, the maximum cluster population was extremely low (4%), suggesting that **Mph3B** does not fold into any specific structures.

Conclusions

The results presented here reveal the power of a modified RaPID system for the ribosomal synthesis of an α/β-helical peptide library and its application for the discovery of SARS-CoV-2 main protease (M^{pro}) inhibitors. One of the peptides, **Mph3**, containing four (1*S*,2*S*)-2-ACPC residues at designated periodical positions, possesses both M^{pro} affinity (K_D = 15.1 nM) and M^{pro} inhibitory activity (IC_{50} = 620 nM, Table 2). Far-UV CD spectroscopy and MD simulation analyses imply that **Mph3** very likely adopt 14-helix-like structure characterized by 11 polar intramolecular contacts (Fig. 6A). Importantly, chloroalkane-tagged **Mph3-ct** exhibits notable cell membrane permeability with a CP_{50} value of 340 nM, comparable to a known membrane permeable peptide, **ct-R9**, which has a CP_{50} of 380 nM (Fig. 5). Despite these favorable

properties, **Mph3** is susceptible to peptidase degradation in serum with half-lives ($t_{1/2}$) of only 2.4 h, resulting in fragmentation at the first two N-terminal residues (Table 2). To address this, we substituted its N-acetyl-D-Tyr residues for its L-counterpart, giving **Mph3y**, an alteration which successfully elevated the serum stability, *i.e.* from $t_{1/2}$ = 2.4 to 11 h. Importantly, **Mph3y** also maintains the favorable K_D/IC_{50} values, as well as cell membrane permeability, of the parental **Mph3**, identifying it as the most promising peptide inhibitor in our study (Table 2 and Fig. 5).

Recently, several studies have identified macrocyclic peptide M^{pro} inhibitors using the RaPID selection.[37–40] Our group reported a novel thioether-macrocyclic peptide M^{pro} inhibitor containing a cyclic γ-amino acid, referred to as GM4 (IC_{50} = 50 nM).[37] Johnsen-Leete *et al.* also reported a thioether-macrocyclic peptide M^{pro} inhibitor (IC_{50} = 70 nM), whose pharmacophore sequence consist of proteinogenic amino acids.[38] However, neither of these macrocyclic peptides showed significant cell membrane permeability. To overcome this issue, the latter group prepared CPP conjugates of the peptide, resulting in antiviral activity in the 10 μM range.[38] There is, however, a discrepancy between the *in vitro* data and cellular data of greater than two orders of magnitude. Harrison *et al.* developed a hydrophobic cyclic peptide M^{pro} inhibitor, M1-5X, with the antiviral activity (EC_{50}) of 13.3 μM. However, conjugation with the CPP resulted in cytotoxicity, thereby preventing further improvement in antiviral activity.[39] These findings indicates that cell membrane permeability remains a major issue.

The α/β-helical peptides developed in this study, **Mph3** and **Mph3y**, contain the backbone hydrogen bond donors and acceptors in the context of their stable helix structures, enabling them to manifest cell permeability in the 300 nM range. Importantly, our work shows that the *de novo* α/β-helical peptides freshly isolated by the RaPID selection can exhibit the desired properties against M^{pro}, giving a potential route for the development of *in vivo* active peptide inhibitors in the future.

Before progressing to check the intracellular inhibitory activities of obtained peptides, two critical issues must be addressed. Firstly, although the **Mph3y** variant of **Mph3** has an improved anti-peptidase/protease stability, it is yet probably insufficiently stable with only a $t_{1/2}$ of 11 h. Though **Mph3-tr2** is near immune to peptidase digestion, its non-specific interaction with serum proteins and poor binding ability to M^{pro} prohibited us from advancing it further. The results with **Mph3y** suggests that a programming for incorporation of unnatural initiators, such as *N*-acetyl-D-Tyr, will generate an initial library that contains active species with better serum stability; we are thus working to redesign the library and selection campaign. Secondly, despite the positive outcomes of this study, **Mph3** shows tight binding to M^{pro} with 15 nM of K_D but its inhibitory activity is limited to an IC_{50} of 620 nM, *i.e.*, there is a ∼40-fold of difference in K_D and IC_{50} values. GM4 shows a ∼8-fold difference between its K_D and IC_{50} values.[37] It is possible that the dimeric nature of M^{pro} relates to the differences in K_D and IC_{50} values. An X-ray structure of the complex of M^{pro} and macrocycle GM4 reveals that the certain critical residues of GM4 bind in a deep pocket at the active site; no helical motif was formed in the M^{pro} complexed GM4 structure. As yet, we do not have an X-ray structure of **Mph3** complexed with M^{pro} which will inform on its binding mode, in particular how deeply the helical motif accesses to the active site and whether or not induced fit occurs on binding. It is possible that the α/β-helical scaffold may be unsuited for potent inhibitors accessing deeply in the active site pocket of M^{pro}. We envision that a library similar to the helix library described in this work can be applied to other targets to test if potent molecules can be obtained for other proteins, with one focus being on induced fit, particularly in targets with known helical binders.[41,42] Nevertheless, the results presented here provide insight that will help in the design of improved α/β-helical peptide libraries.

In conclusion, we have designed and generated an α/β-helical peptide library *via* genetic code reprogramming that enables installation of up to five cyclic β-amino acids at designated positions. The RaPID selection using this library against SARS-CoV-2 M^{pro} yielded peptides containing up to four (1*S*,2*S*)-2-ACPC residues, one of which exhibited both M^{pro} inhibitory activity (IC_{50} = 620 nM) and cell membrane permeability (CP_{50} = 340 nM). These results show for the first time that *de novo* α/β-helical peptides can be discovered from such a library against a protein target of choice, opening an avenue for simultaneously identifying drug-like peptides with target binding/inhibitory ability and cell membrane permeability/proteolytic stability properties. This is an important advance because optimizing cell membrane permeability for (cyclic) α-peptides, even when they have very high target affinity, is often time-consuming, if possible at all.

Experimental

Preparation of flexizymes and tRNAs

Flexizymes (dFx, eFx) and tRNAs ($tRNA^{ini}_{CAU}$, $tRNA^{Pro1E2}_{CAU}$) were prepared by *in vitro* transcription using the T7 RNA polymerase. Template DNAs with an upstream T7 promoter sequence were prepared by the extension of forward and reverse extension primers followed by PCR amplification using forward and reverser PCR primers [RNA and primer sequences are shown in Table S1(a), ESI†]. PCR products were purified by phenol-chloroform extraction and ethanol precipitation. The purified DNAs were *in vitro* transcribed overnight at 37 °C in the reaction mixture [40 mM Tris–HCl (pH 8.0), 22.5 mM $MgCl_2$, 1 mM dithiothreitol, 1 mM spermidine, 0.01% Triton X-100, 0.12 μM T7 polymerase, 0.04 U μL^{-1} RNasin RNase inhibitor (Promega), 3.75 mM NTPs (pH 8.0)]. The DNA in the transcription mixture was degraded by RQ1 DNase (Promega) treatment for 1 h at 37 °C. The resulting RNAs were purified by 12% (for flexizymes) or 8% (for tRNAs) polyacrylamide gel containing 6 M urea.

Preparation of aminoacyl-tRNAs

(1*S*,2*S*)-2-ACPC and ^{Ac}Tyr were preactivated as their 3,5-dinitrobenzyl ester (DBE) and cyanomethyl ester (CME), respectively, according to reported methods.[17,25] These amino acids were then used for the tRNA aminoacylation reaction ($tRNA^{Pro1E2}_{CAU}$ for

(1*S*,2*S*)-2-ACPC, $tRNA^{ini}_{CAU}$ for ^{Ac}Tyr) using the corresponding flexizymes (dFx for DBE, eFx for CME) Reaction was carried out at 4 °C for 2 h (for ^{Ac}Tyr) and 22 h [for (1*S*,2*S*)-2-ACPC] in 600 mM $MgCl_2$, 50 mM each buffer [Bicine pH 8.7 for (1*S*,2*S*)-2-ACPC, HEPES-KOH pH 7.5 for ^{Ac}Tyr]. The reaction products were purified by ethanol precipitation, then washed twice with 70% ethanol in 0.3 M AcONa and once with 70% ethanol. The resulting aminoacyl-tRNA pellets were air-dried for 5 minutes and dissolved in 1 mM AcONa immediately before use.

Preparation of mRNA library encoding α/β-helical peptides

mRNA libraries encoding α/β-helical peptides were prepared by *in vitro* transcription using the T7 RNA polymerase. Template DNAs with an upstream T7 promoter sequence were prepared by the extension of forward and reverse extension primers followed by PCR amplification using forward and reverser PCR primers (RNA and primer sequences are shown in Table S1(a), ESI†). PCR products were purified by phenol-chloroform extraction and ethanol precipitation. The purified DNAs were *in vitro* transcribed overnight at 37 °C in the reaction mixture (40 mM Tris–HCl (pH 8.0), 22.5 mM $MgCl_2$, 1 mM dithiothreitol, 1 mM spermidine, 0.01% Triton X-100, 0.12 μM T7 polymerase, 0.04 U μL^{-1} RNasin RNase inhibitor (Promega), 3.75 mM NTPs (pH 8.0)). DNA in the transcription mixture was degraded by RQ1 DNase (Promega) treatment for 1 h at 37 °C. The resulting RNAs were purified by 8% polyacrylamide gel containing 6 M urea, extracted in 0.3 M NaCl, and collected by ethanol precipitation. The purified RNAs were dissolved in ultrapure water to a final concentration of 10 μM.

Translation of α/β-helical peptides

DNA and mRNA libraries (DNA, RNA and primer sequences are shown in Table S1(b), ESI†) were translated using FIT system for 30 min at 37 °C using the following conditions: 50 mM HEPES-KOH (pH 7.6), 100 mM KOAc, 2 mM GTP, 2 mM ATP, 1 mM CTP, 1 mM UTP, 20 mM creatine phosphate, 2 mM spermidine, 2 mM DTT, 12.3 mM $Mg(OAc)_2$, 1.5 mg mL^{-1} *E. coli* total tRNA, 1.2 μM ribosome, 0.6 μM MTF, 4 μg mL^{-1} creatine kinase, 3 μg mL^{-1} Myokinase, 0.1 μM pyrophosphatase, 0.1 μM nucleotide-diphosphatase kinase, 0.1 μM T7 RNA polymerase, 20 μM EF-Tu/EF-Ts, 0.73 μM AlaRS, 0.03 μM ArgRS, 0.38 μM AsnRS, 0.13 μM AspRS, 0.02 μM CysRS, 0.09 μM GlyRS, 0.4 μM IleRS, 0.04 μM LeuRS, 0.11 μM LysRS, 0.68 μM PheRS, 0.16 μM ProRS, 0.04 μM SerRS, 0.09 μM ThrRS, 0.02 μM TyrRS, 0.02 μM ValRS, 0.25 μM RF2, 0.17 μM RF3, 0.5 μM RRF, 2.7 μM IF1, 3 μM IF2, 1.5 μM IF3, 0.1 μM EF-G, 5 mM each α-amino acid (A, R, N, D, C, G, I, L, K, F, P, S, T, Y, and V), 50 μM each pre-charged aminoacyl-tRNA, and 1 μM mRNA library. 50 μM ^{Ac}Tyr-$tRNA^{ini}_{CAU}$ for the initiator AUG codon and 50 μM (1*S*,2*S*)-2-ACPC-$tRNA^{Pro1E2}_{CAU}$ for elongator AUG codons were added in the translation mixture.

Expression and purification of recombinant SARS-CoV-2 M^{pro}

SARS-CoV-2 M^{pro} was prepared as reported,[30] and assays were performed exclusively using freshly purified recombinant M^{pro} solution.

RaPID selection of peptides against SARS-CoV-2 M^{pro}

The mRNA library encoding α/β-helical peptides was ligated with puromycin-linker at the 3′-end. The puromycin-ligated mRNA library was then translated for 30 min at 37 °C in a final volume of 150 μL (for the first round of selection) and in a final volume of 5 μL (for the second to sixth round of selection) scale. Puromycin ligated to 3′-end of mRNA was conjugated at C-terminus of corresponding translated peptides by incubation for 12 min at 25 °C. 1 μL of 100 mM EDTA (pH 8.0) was added to quench the translation reaction. The resulting mRNA–peptide conjugates were then reverse transcribed at 42 °C for 15 min with M-MLV reverse transcriptase lacking RNase H activity (Promega) and TGVTNG·R34 primer (5′-TTTCCGCCCCCCGT CCTAACCGTTAGTCACACCCGT-3′). Before the affinity-based selection, Avi-tagged M^{pro} was immobilized on the Dynabeads M-280 Streptavidin (Thermo Fisher). The mRNA/cDNA–peptide conjugates were applied to M^{pro}-immobilized Dynabeads and incubated at 4 °C for 15 min (positive selection). For the 2nd to 6th round of selection, beads binding peptides were removed from mRNA/cDNA–peptide libraries (negative selection) by mixing the same volume of negative beads and collecting the supernatant for three times before the positive selection. The beads used for positive selection and 3rd negative selection were then collected and washed with 100 μL of TBS-T buffer (50 mM Tris–HCl (pH 7.6), 150 mM NaCl, 0.05%$_{v/v}$ Tween20) three times. cDNA was eluted from the beads in 300 μL (for 1st round) or 100 μL (for second to sixth round) of PCR buffer (10 mM Tris–HCl (pH 9.0), 50 mM KCl, 0.1%$_{v/v}$ Triton X-100, 0.25 mM dNTP, 2.5 mM $MgCl_2$, 0.25 μM T7·F52 primer (5′-GGCGTAATACGACTCACTATAGGGTTGAACTTTAAGTAGGA GATATATCCAT-3′) and 0.25 μM TGVTNG·R34 primer) at 95 °C for 5 min. 1 μL of the eluate was taken and mixed with 19 μL of 1× PCR buffer that contained 0.002%$_{v/v}$ SYBR green I in DMSO and 1.5%$_{v/v}$ *Taq* DNA polymerase for the quantification of cDNA by real-time PCR. The PCR amplification of cDNA in the rest eluate was conducted by adding 1.5%$_{v/v}$ *Taq* DNA polymerase, followed by phenol/chloroform extraction and ethanol precipitation. The resulting DNA was dissolved in 50 mM KCl and used for *in vitro* transcription in reaction mixture (40 mM Tris–HCl (pH 8.0), 22.5 mM $MgCl_2$, 1 mM dithiothreitol, 1 mM spermidine, 0.01% Triton X-100, 0.12 μM T7 polymerase, 0.04 U μL^{-1} RNasin RNase inhibitor (Promega), 3.75 mM NTPs (pH 8.0)) overnight at 37 °C and purified for the subsequent round of selection.

Synthesis of α/β-helical peptides

NovaPEG Fmoc Rink Amide resin was added to a 5 mL tube and swelled by DMF. An automatic peptide synthesizer, Syro I, was used for the elongation of peptide sequences. The peptide N-terminus was acetylated using 250 μL of 0.5 M acetic anhydride/0.25 M DIPEA in NMP. The resins were washed with CH_2Cl_2 and air-dried. Peptides were then cleaved and deprotected by adding 3 mL of a universal cleavage mixture consisting of the ratio of TFA : TIS : DODT : H_2O = 92.5 : 2.5 : 2.5 : 2.5. Crude peptide solutions were separated from the resins by

filtration and collected in 15 mL tubes. The solutions were applied to centrifugal evaporator to remove TFA. 15 mL of diethyl ether was added to the residues and precipitations were washed with 5 mL of diethyl ether five times and air-dried. The precipitations were dissolved in 5 mL of DMSO. Crude peptide solutions were filtered with 0.45 μm filter and purified by HPLC. Acetonitrile was removed from the fractions using centrifugal evaporator and subsequently the fractions were lyophilized. Peptides were dissolved in DMSO and their concentrations were measured by UV-spectroscopy.

Surface plasmon resonance binding analyses

The binding affinities of the chemically synthesized α/β-helical peptides against M^{pro} were evaluated by surface plasmon resonance (SPR) using a Biacore T200 machine (Cytiva). Avi-tagged M^{pro} was immobilized on a Biotin CAPture Chip (Cytiva) to an immobilization level of 1800–2000 response units (RU) using the standard immobilization protocol. Single-cycle kinetics were measured using a five-point, two-fold serial dilution (spanning a range of 1000 nM to 62.5 nM) in running buffer consisting of 50 mM Tris–HCl (pH 7.6), 150 mM NaCl, 0.05%$_{v/v}$ Tween 20, 2%$_{v/v}$ DMSO at a flow rate of 30 μL min^{-1}. Reference flow-cell was subtracted and the resulting sensorgrams were fitted to a 1 : 1 binding model using a Biacore evaluation software.

Inhibition assays

Solid-phase extraction (SPE) coupled with mass spectrometry assays were performed as described.[30] Inhibition of the activity of isolated recombinant SARS-CoV-2 M^{pro} with the final concentration of 75/50 nM was monitored by measuring the percentage hydrolysis of the 11-mer substrate TSAVLQ/SGFRKMAFPS-NH_2 in the presence of variable concentrations of helical peptides.

Circular dichroism analyses

Peptide samples were dried and dissolved in 50%$_{v/v}$ 2,2,2-trifluoroethanol in 10 mM phosphate buffer (pH 8.0) to a concentration of 75 μM, and all samples were measured using a sample cell of 2 mm path length and JASCO J-1000 spectrometer. Baseline spectra recorded with buffer were subtracted from the raw data. Dissolved samples were then measured at 25 °C with 6 times accumulation. Data were converted to ellipticity (deg cm^2 dmol^{-1} res^{-1}) according to the following equation:

$$[\theta] = [\theta]_{obs} \cdot A/(l \cdot C)$$

where $[\theta]_{obs}$ (deg) is the CD signal, A (mol dm^{-3} res^{-1}) is the molecular weight divided by the number of amino acid residues, l (dm) is the path length, and C (mol dm^{-3}) is the concentration.

Serum stability assays

10 μM synthetic macrocyclic peptides (**Mph3**, **Mph3A**, **Mph3B**, **Mph3y**, **Mph5**, **Mph5A**, **Mph5B**) were co-incubated with 10 μM internal standard peptide (NH_2-PEG_5-^{D}W^{D}S^{D}T^{D}N^{D}D^{D}W^{D}S^{D}T^{D}N^{D}D-PEG_5-$CONH_2$) in human serum (Cosmo Bio) at 37 °C for up to 24 h. 9 μL of the mixture was sampled at each time point (0, 0.5, 1, 2, 4, 6, and 24 h), and protease reaction was quenched by methanol precipitation. 10 μL of the supernatant was mixed with 90 μL of 1%$_{v/v}$ TFA and centrifuged at 15 310 G, 25 °C, for 3 min. The supernatant was collected for liquid chromatography/mass spectrometry analysis with a reverse-phase column (ACQUITY UPLC BEH C18 Column, 130 Å, 1.7 μm, 2.1 × 150 mm; Waters) and a Xevo G2-XS QTof system (Waters) with a linear gradient from 1% to 60% buffer B. Buffer A was H_2O with 0.1%$_{v/v}$ formic acid and buffer B was CH_3CN with 0.1%$_{v/v}$ formic acid.

Chloroalkane penetration assay (CAPA)

Cell penetration assays using CAPA were carried out according to the protocols of Perato *et al.*[36] HaloTag-GFP-Mito cells used for the assay were HEK293 cells. Cell lines were generated in the laboratory and cultured using DMEM (High Glucose) (Nacalai Tesque) + 10% heat-inactivated FBS + 1% Pen/Strep and kept at 37 °C with 5% CO_2. Cells were seeded in Collagen-Coated Microplate 96 well with Lid Collagen Type I (IWAKI) at a density of 4 × 10^4 cells per well before the day of the experiment. After the attraction of DMEM buffer in each well, peptide solutions dissolved in Opti-MEM®I (1×) (Nacalai Tesque) + 5%$_{v/v}$ FBS containing 1% DMSO$_{v/v}$ were added, followed by 24 h incubation at 37 °C with 5% CO_2. Cells were washed by 15 min incubation in Opti-MEM + 5% FBS after attracting peptide solutions, and then incubated with 5 μM ct-TAMRA dissolved in Opti-MEM + 5% FBS containing 0.5%$_{v/v}$ DMSO for 15 min. After removing the media containing ct-TAMRA, the cells were rinsed twice with Opti-MEM + 5% FBS. The cells were trypsinized and resuspended in PBS and then the fluorescence of GFP and ct-TAMRA was measured by CytoFLEX S flow cytometer (Beckman Coulter). All assays were performed in triplicate.

Structural calculation using molecular dynamics simulation

The crystallographically-observed helical structures of α/β-helical peptides, including an (1*S*,2*S*)-2-ACPC-containing ααβ peptide (PDB 3C3H) and an αααβ peptide (PDB 3C3F),[31] provided structural templates for the *in silico* modeling of the peptides in this work. Peptide models were constructed by modifying sequences to match the peptides of interest, using the mutagenesis tool in PyMOL (v. 2.3.0).[43] The most favorable backbone-dependent rotamer for each residue was selected.[44] The structures of the α-Ala- or β-Ala-substituted peptide analogs were prepared by removal of atoms from (1*S*,2*S*)-2-ACPC. Molecular mechanics (MM) parameters were taken from the Amber ff99SB-ILDN force field,[45] except for the charges of the non-standard β-amino acids [(1*S*,2*S*)-2-ACPC and β-Ala] which were calculated using the RESP protocol (Fig. S13 and S14, ESI†).[46,47]

Simulations were performed using pmemd (Amber20).[48] Each peptide was placed in a periodic octahedral simulation box with a 1.1 nm minimum distance from the box edges and solvated with TIP3P water molecules.[49] The system was neutralized by addition of Na^+/Cl^- ions, then subjected to a 1000-step steepest descent MM energy minimization, resulting in a geometrically reasonable helical peptide structure free of

unfavorable clashes. The system was then for 200 ps in the NVT ensemble (1 kcal mol^{-1} $Å^{-2}$ restraint on nonhydrogen atoms), using a 2 fs time steps and with hydrogen-containing bonds constrained by SHAKE.[50] The temperature of the system was maintained at 298.15 K using the Langevin thermostat with a collision frequency of (1 ps^{-1}). This was followed by 200 ps unrestrained MD simulations in the NPT at 298.15 K and 1 bar (Berendsen barostat with a relaxation time of 2 ps)[51] and further unrestrained NVT relaxation (4.6 ns). Peptide conformational sampling was performed in triplicate using the Gaussian accelerated MD protocol,[52] with a total simulation length of 504.6 ns, consisting of 2 ns conventional MD (first 400 ps used as preparation), 2.6 ns boosted MD (first 400 ps as preparation), and 500 ns production phase. Dual boost on both dihedral and total potential energies (σ_0 = 6 kcal mol^{-1}) was applied with thresholds set to the lower bounds. Long-range electrostatic interactions were calculated using Particle Mesh Ewald.[53] The sampled peptide coordinates were analyzed using GROMACS tools (v. 2019.2),[54] including clustering (15 000 structures per peptide) with a 3 Å Cα RMSD cut-off by the gromos algorithm.[55] Secondary structure was assigned by DSSP (v. 2.0.4).[56,57] PyMOL (v. 2.3.0)[43] was used for analysis and visualization of peptide structures and polar contacts. Note that the environment for the MD simulations were performed in aqueous solution, whereas the CD measurements were performed in 50%$_{v/v}$ TFE due to the relatively low water solubility of peptides.

Author contributions

M. K., T. K. conceived the study. M. K., T. R. M., H. T. H. C., A. T., L. B., E. S., N. T. planned and performed the experiments. M. K., T. R., H. T. H. C., L. B., T. K., A. K., C. J. S., F. D., and H. S. wrote the manuscript.

Data availability

The data supporting this article have been included as part of the ESI.†

Conflicts of interest

There are no conflicts to declare.

Acknowledgements

This work was supported by Japan Society for the Promotion of Science (JSPS) Grant-in-Aid for JSPS Fellows (21J11468) to M. K.; Grant-in-Aid for Scientific Research (A) (22H00439) and Grant-in-Aid for Challenging Research (Pioneering) (21K18233 and 24K21267) to T. K.; Grant-in-Aid for Specially Promoted Research (20H05618) to H. S.

Notes and references

1 T. Katsu, M. Kuroko, T. Morikawa, K. Sanchika, H. Yamanaka, S. Shinoda and Y. Fujita, *Biochim. Biophys. Acta*, 1990, **1027**, 185–190.
2 K. K. Hou, H. Pan, G. M. Lanza and S. A. Wickline, *Biomaterials*, 2013, **34**, 3110–3119.
3 K. T. O'Neil and W. F. DeGrado, *Trends Biochem. Sci.*, 1990, **15**, 59–64.
4 W. N. Hait, L. Grais, C. Benz and E. C. Cadman, *Cancer Chemother. Pharmacol.*, 1985, **14**, 202–205.
5 M. Moreno and E. Giralt, *Toxins*, 2015, **7**, 1126–1150.
6 M. J. I. Andrews and A. B. Tabor, *Tetrahedron*, 1999, **55**, 11711–11743.
7 G. L. Verdine and G. J. Hilinski, *Methods Enzymol.*, 2012, **503**, 3–33.
8 C. Cabrele, T. A. Martinek, O. Reiser and Ł. Berlicki, *J. Med. Chem.*, 2014, **57**, 9718–9739.
9 S. H. Gellman, *Acc. Chem. Res.*, 1998, **31**, 173–180.
10 B. F. Fisher, S. H. Hong and S. H. Gellman, *J. Am. Chem. Soc.*, 2018, **140**, 9396–9399.
11 L. M. Johnson and S. H. Gellman, *Methods Enzymol.*, 2013, **523**, 407–429.
12 M. A. Schmitt, S. H. Choi, I. A. Guzei and S. H. Gellman, *J. Am. Chem. Soc.*, 2006, **128**, 4538–4539.
13 S. H. Choi, I. A. Guzei, L. C. Spencer and S. H. Gellman, *J. Am. Chem. Soc.*, 2009, **131**, 2917–2924.
14 M. A. Schmitt, B. Weisblum and S. H. Gellman, *J. Am. Chem. Soc.*, 2007, **129**, 417–428.
15 M. D. Boersma, H. S. Haase, K. J. Peterson-Kaufman, E. F. Lee, O. B. Clarke, P. M. Colman, B. J. Smith, W. S. Horne, W. D. Fairlie and S. H. Gellman, *J. Am. Chem. Soc.*, 2012, **134**, 315–323.
16 J. W. Checco, E. F. Lee, M. Evangelista, N. J. Sleebs, K. Rogers, A. Pettikiriarachchi, N. J. Kershaw, G. A. Eddinger, D. G. Belair, J. L. Wilson, C. H. Eller, R. T. Raines, W. L. Murphy, B. J. Smith, S. H. Gellman and W. D. Fairlie, *J. Am. Chem. Soc.*, 2015, **137**, 11365–11375.
17 H. Murakami, A. Ohta, H. Ashigai and H. Suga, *Nat. Methods*, 2006, **3**, 357–359.
18 Y. Goto, T. Katoh and H. Suga, *Nat. Protoc.*, 2011, **6**, 779–790.
19 T. Katoh, Y. Iwane and H. Suga, *Nucleic Acids Res.*, 2017, **45**, 12601–12610.
20 T. Katoh and H. Suga, *J. Am. Chem. Soc.*, 2018, **140**, 12159–12167.
21 T. Dale and O. C. Uhlenbeck, *Trends Biochem. Sci.*, 2005, **30**, 659–665.
22 T. Dale, L. E. Sanderson and O. C. Uhlenbeck, *Biochemistry*, 2004, **43**, 6159–6166.
23 T. Katoh, I. Wohlgemuth, M. Nagano, M. V. Rodnina and H. Suga, *Nat. Commun.*, 2016, **7**, 11657.
24 T. Katoh and H. Suga, *J. Am. Chem. Soc.*, 2020, **142**, 16518–16522.
25 T. Katoh, T. Sengoku, K. Hirata, K. Ogata and H. Suga, *Nat. Chem.*, 2020, **12**, 1081–1088.

26 T. Katoh and H. Suga, *BCSJ*, 2021, **94**, 549–557.
27 Y. Yamagishi, I. Shoji, S. Miyagawa, T. Kawakami, T. Katoh, Y. Goto and H. Suga, *Chem. Biol.*, 2011, **18**, 1562–1570.
28 T. Fujino, Y. Goto, H. Suga and H. Murakami, *J. Am. Chem. Soc.*, 2016, **138**, 1962–1969.
29 P. V'kovski, A. Kratzel, S. Steiner, H. Stalder and V. Thiel, *Nat. Rev. Microbiol.*, 2021, **19**, 155–170.
30 T. R. Malla, A. Tumber, T. John, L. Brewitz, C. Strain-Damerell, C. D. Owen, P. Lukacik, H. T. H. Chan, P. Maheswaran, E. Salah, F. Duarte, H. Yang, Z. Rao, M. A. Walsh and C. J. Schofield, *Chem. Commun.*, 2021, **57**, 1430–1433.
31 W. S. Horne, J. L. Price and S. H. Gellman, *Proc. Natl. Acad. Sci. U. S. A.*, 2008, **105**, 9151–9156.
32 N. J. Greenfield, *Nat. Protoc.*, 2006, **1**, 2876–2890.
33 D. Roccatano, G. Colombo, M. Fioroni and A. E. Mark, *Proc. Natl. Acad. Sci. U. S. A.*, 2002, **99**, 12179–12184.
34 K. J. Peterson-Kaufman, H. S. Haase, M. D. Boersma, E. F. Lee, W. D. Fairlie and S. H. Gellman, *ACS Chem. Biol.*, 2015, **10**, 1667–1675.
35 W. S. Horne, L. M. Johnson, T. J. Ketas, P. J. Klasse, M. Lu, J. P. Moore and S. H. Gellman, *Proc. Natl. Acad. Sci. U. S. A.*, 2009, **106**, 14751–14756.
36 L. Peraro, K. L. Deprey, M. K. Moser, Z. Zou, H. L. Ball, B. Levine and J. A. Kritzer, *J. Am. Chem. Soc.*, 2018, **140**, 11360–11369.
37 T. Miura, T. R. Malla, C. D. Owen, A. Tumber, L. Brewitz, M. A. McDonough, E. Salah, N. Terasaka, T. Katoh, P. Lukacik, C. Strain-Damerell, H. Mikolajek, M. A. Walsh, A. Kawamura, C. J. Schofield and H. Suga, *Nat. Chem.*, 2023, **15**, 998–1005.
38 J. Johansen-Leete, S. Ullrich, S. E. Fry, R. Frkic, M. J. Bedding, A. Aggarwal, A. S. Ashhurst, K. B. Ekanayake, M. C. Mahawaththa, V. M. Sasi, S. Luedtke, D. J. Ford, A. J. O'Donoghue, T. Passioura, M. Larance, G. Otting, S. Turville, C. J. Jackson, C. Nitsche and R. J. Payne, *Chem. Sci.*, 2022, **13**, 3826–3836.
39 K. Harrison, P. W. Carlos, S. Ullrich, A. Aggarwal, J. Johansen-Leete, V. M. Sasi, I. Barter, J. W. C. Maxwell, M. J. Bedding, M. Larance, S. Turville, A. Norman, C. J. Jackson, C. Nitsche and R. J. Payne, *Chemistry*, 2024, e202401606.
40 Y. Tan, J. Yang, M. Wang, Q. Peng, Y. Li, L. Fu, M. Zhang, J. Wu, G. Yang, C. J. Hipolito, Y. Zhang, J. Qi, Y. Shi and Y. Yin, *J. Med. Chem.*, 2024, **67**, 20258–20274.
41 Y. Mesrouze, H. Gubler, F. Villard, R. Boesch, J. Ottl, J. Kallen, P. C. Reid, C. Scheufler, A. L. Marzinzik and P. Chène, *ACS Chem. Biol.*, 2023, **18**, 643–651.
42 F. Hink, J. Aduriz-Arrizabalaga, X. Lopez, H. Suga, D. De Sancho and J. M. Rogers, *J. Am. Chem. Soc.*, 2024, **146**, 24348–24357.
43 *The PyMOL Molecular Graphics System, Version 2.3.0*, Schrödinger LLC.
44 R. L. Dunbrack Jr and F. E. Cohen, *Protein Sci.*, 1997, **6**, 1661–1681.
45 K. Lindorff-Larsen, S. Piana, K. Palmo, P. Maragakis, J. L. Klepeis, R. O. Dror and D. E. Shaw, *Proteins*, 2010, **78**, 1950–1958.
46 C. I. Bayly, P. Cieplak, W. Cornell and P. A. Kollman, *J. Phys. Chem.*, 1993, **97**, 10269–10280.
47 W. D. Cornell, P. Cieplak, C. I. Bayly and P. A. Kollman, *J. Am. Chem. Soc.*, 1993, **115**, 9620–9631.
48 D. A. Case, H. M. Aktulga, K. Belfon, D. S. Cerutti, G. A. Cisneros, V. W. D. Cruzeiro, N. Forouzesh, T. J. Giese, A. W. Götz, H. Gohlke, S. Izadi, K. Kasavajhala, M. C. Kaymak, E. King, T. Kurtzman, T.-S. Lee, P. Li, J. Liu, T. Luchko, R. Luo, M. Manathunga, M. R. Machado, H. M. Nguyen, K. A. O'Hearn, A. V. Onufriev, F. Pan, S. Pantano, R. Qi, A. Rahnamoun, A. Risheh, S. Schott-Verdugo, A. Shajan, J. Swails, J. Wang, H. Wei, X. Wu, Y. Wu, S. Zhang, S. Zhao, Q. Zhu, T. E. Cheatham 3rd, D. R. Roe, A. Roitberg, C. Simmerling, D. M. York, M. C. Nagan and K. M. Merz Jr, *J. Chem. Inf. Model.*, 2023, **63**, 6183–6191.
49 W. L. Jorgensen, J. Chandrasekhar, J. D. Madura, R. W. Impey and M. L. Klein, *J. Chem. Phys.*, 1983, **79**, 926–935.
50 J.-P. Ryckaert, G. Ciccotti and H. J. C. Berendsen, *J. Comput. Phys.*, 1977, **23**, 327–341.
51 H. J. C. Berendsen, J. P. M. Postma, W. F. van Gunsteren, A. DiNola and J. R. Haak, *J. Chem. Phys.*, 1984, **81**, 3684–3690.
52 Y. Miao, V. A. Feher and J. A. McCammon, *J. Chem. Theory Comput.*, 2015, **11**, 3584–3595.
53 T. Darden, D. York and L. Pedersen, *J. Chem. Phys.*, 1993, 10089–10092.
54 M. J. Abraham, T. Murtola, R. Schulz, S. Páll, J. C. Smith, B. Hess and E. Lindahl, *SoftwareX*, 2015, **1–2**, 19–25.
55 X. Daura, K. Gademann, B. Jaun, D. Seebach, W. F. van Gunsteren and A. E. Mark, *Angew. Chem., Int. Ed.*, 1999, **38**, 236–240.
56 W. G. Touw, C. Baakman, J. Black, T. A. H. te Beek, E. Krieger, R. P. Joosten and G. Vriend, *Nucleic Acids Res.*, 2015, **43**, D364–D368.
57 R. P. Joosten, T. A. H. te Beek, E. Krieger, M. L. Hekkelman, R. W. W. Hooft, R. Schneider, C. Sander and G. Vriend, *Nucleic Acids Res.*, 2011, **39**, D411–D419.